Plasma Phys. Control. Fusion **51** (2009) 015007 (12pp) doi:10.1088/0741-3335/51/1/015007

Expanding hydrogen plasmas: photodetachment-technique diagnostics

Zh Kiss'ovski[1], St Kolev[1], S Müller[2], Ts Paunska[1], A Shivarova[1] and Ts Tsankov[1]

[1] Faculty of Physics, Sofia University, BG-1164 Sofia, Bulgaria
[2] Institut für Experimentalphysik V, Ruhr-University Bochum, D-44780, Germany

E-mail: ashiva@phys.uni-sofia.bg

Received 16 June 2008, in final form 13 October 2008
Published 4 December 2008
Online at stacks.iop.org/PPCF/51/015007

Abstract

The laser photodetachment technique in its combination with probe measurements is applied for the determination of the electronegativity and the concentration of the negative hydrogen ions in the expansion plasma volume of an inductively driven two-chamber plasma source. Both the implementation of the method and the obtained results are discussed in the study. The variations of the gas pressure and the applied rf power in the experiments are in the ranges $p = (0.3–5)$ Pa and $P = (200–700)$ W, respectively. The results for an almost constant—with the gas pressure—electronegativity and its increase with the applied power are in agreement with theoretical estimations. The obtained nonmonotonic variation of the concentration of the negative ions with increasing gas pressure correlates with the gas pressure dependence of the electron density in the expansion plasma region of the source.

(Some figures in this article are in colour only in the electronic version)

1. Introduction

The current development towards ITER motivates active research on negative hydrogen ion beam sources which—due to the size of the new fusion reactor—are the only possibility for additional plasma heating through high-energetic neutral beam injection. The confidence that employing rf sources of negative ion beams is a better solution compared with the arc sources stimulates the research on inductively driven sources [1, 2]. As is known, the construction of the sources—both rf and arc sources—is of the type of tandem plasma sources [3, 4] which ensures space separation in the source of regions of high- and low- energetic electrons favouring the two step reaction for production of negative hydrogen ions via dissociative attachment of electrons to vibrationally excited molecules. Moreover, the discharge vessel of the rf sources [1, 2]

of negative hydrogen ions consists of two chambers of different sizes. In the first smaller-size chamber the driver—the region of the rf power deposition—is located, and the second bigger-size chamber where the magnetic filter for electron cooling and the extraction region are located is a volume for plasma expansion from the driver.

Both the complicated configuration of the discharge vessel and the regime of the discharge maintenance in the source make the theoretical description of the source a tricky task which requires covering many aspects—moreover, within at least 2D discharge modelling [5, 6]—such as (i) a detailed description of the particle fluxes which are shown [7, 8] to ensure the plasma existence in the expanding plasma region (i.e. in the second chamber), (ii) plasma expansion through a magnetic filter [9–12], (iii) description of the free-fall regime of discharge maintenance in hydrogen [13–15] which in inductive discharges is accompanied by stochastic heating [16–19] as well as (iv) extended knowledge on the particle impact processes in hydrogen [20–22]. Due to the complexity of the problem, regardless of the extensive research and the profound knowledge accumulated, a complete model of the operation of the source as a whole is still missing. Along these lines, the experiments on the discharge diagnostics in the sources are very crucial in giving directions for the discharge modelling and for the optimization of the discharge conditions.

Certainly, the extracted negative ion current is the most important output parameter of the source. Therefore, the main experimental work has been directed towards its measurement [1, 23–26] combined with probe diagnostics [27, 28] and optical emission spectroscopy diagnostics [29] carried out mainly in the expanding plasma region around the magnetic filter for electron cooling. Since the concentration of the negative ions is the other important parameter of the source which correlates with the density of the extracted negative ion current, extended research has been carried out in this direction including the development of specific diagnostic techniques. The laser photodetachment technique suggested and developed by Bacal [30–32] is the most remarkable and reliable contribution to the topic.

Carrying out plasma diagnostics in the big ion beam sources developed directly for fusion applications runs into trouble due to the limited access of the diagnostic tools to the different regions of the source. This motivates the experiments in small size plasma sources, such as the source studied here, which are flexible regarding the experimental arrangements for the discharge diagnostics. Recent experiments by probe diagnostics [33–35] carried out at the same set-up (measurements of the spatial distribution of plasma characteristics in the expansion plasma region of the source and their redistribution due to a magnetic filter inserted therein) have given an indication of the mechanisms of the plasma expansion from the driver into the second chamber of the source as well as of the mechanisms governing the operation of the magnetic filter.

This study presents experiments based on the laser photodetachment technique, combined with probe diagnostics, for the determination of the electronegativity and of the concentration of the negative hydrogen ions in the expansion plasma volume of a two-chamber inductively driven plasma source. The gas pressure p and the applied rf power P have been varied in the experiments, in the ranges $p = (0.3–5)$ Pa and $P = (200–700)$ W. In addition to the obtained results, the use of the method is also stressed (on experimental arrangements as well as the influence of the laser pulse energy and of the laser beam diameter on the photodetachment signal). The results for an almost constant—with the gas pressure—electronegativity and its increase with the applied power are in agreement with theoretical estimations. The value of the gas pressure obtained in the experiment as an optimum one regarding a maximum concentration of the negative ions correlates with the gas pressure variation of the electron density.

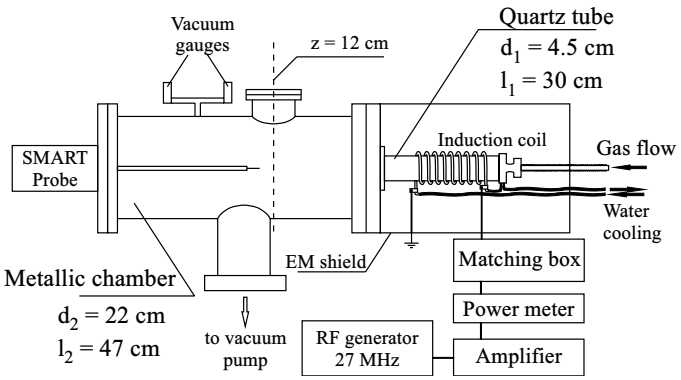

Figure 1. Schematic representation of the two-chamber plasma source. The position (marked by a dashed line) where the photodetachment measurements are performed is 12 cm away from the transition between the two chambers.

2. Experimental arrangements

The plasma source (figure 1) is the same as described before [33–36]: an inductively driven discharge in a two-chamber vessel. The latter consists of a quartz tube (with a diameter of 4.5 cm and a length of 30 cm) where the rf power deposition is located and a metallic chamber (radius of 11 cm and length of 47 cm) provides the volume for plasma expansion from the first chamber. The inductive driving of the discharge is via a 9-turn cylindrical copper coil closely wound on the quartz tube. A rf signal from a high-frequency oscillator ICOM IC-718 (frequency range 1.8–29.7 MHz) after amplification by a linear amplifier ACOM 2000A (output power up to 1.5 kW), fed to the coil through a matching box, produces the discharge. The rf power is monitored by a Rohde and Schwarz NRT powermeter (with NAP-Z8 measuring sensor). A turbomolecular pumping station TurboCube TSU 521 with a membrane forevacuum pump ensures the vacuum in the system. The gas flow is controlled by MKS Mass-Flo flowmeter.

The discharge is in a hydrogen gas, operating at a frequency of 27 MHz. In the experiments the gas pressure variation is between 0.3 and 5 Pa. The power delivered to the plasma (forward minus reflected power) is in the range $P = (200–700)$ W.

The measurements of the plasma parameters (electron density and temperature) are performed by using a SmartProbe^{TM} probe system with a probe movable in the axial direction (along the length of the discharge vessel). The probe tip is a tungsten wire (0.38 mm in diameter, with a length of 1 cm). The system has a built-in passive compensation of the influence of the rf field on the probe characteristics. Each probe characteristic is obtained by averaging over 45 probe voltage sweeps. The measurements are in the second chamber of the source, covering also 2 cm of the quartz tube. The ABR probe theory [37, 38] is applied to process the probe characteristics, as it has been used before [35, 39].

The photodetachment measurements of the negative hydrogen ion concentration stressed here are performed 12 cm away from the quartz tube end, in the region of plasma expansion. The axial position of the measurements is marked in figure 1 with a dashed line. Figure 2 presents a cross-sectional view of the source together with the set-up for registration of the photodetachment signal. The second harmonic radiation ($\lambda = 532$ nm) of a Surelite III-10 Nd : YAG laser is used to irradiate the plasma and detach the electrons from the negative ions. The laser is able to deliver up to 425 mJ per pulse with a repetition frequency of 10 Hz. The

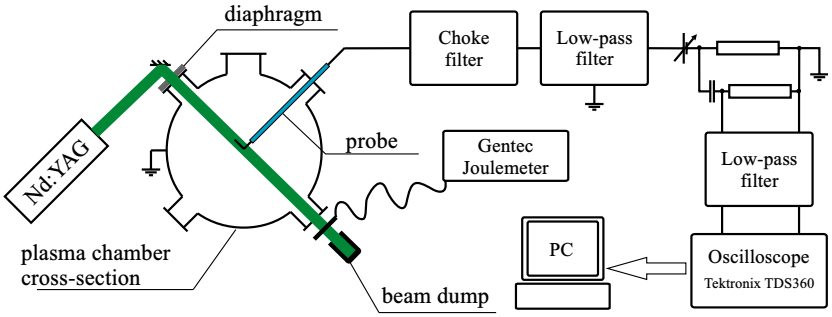

Figure 2. Arrangement for the laser photodetachment technique diagnostics: positions of the laser beam and of the probe detecting the excess electrons as well as schematic representation of the set-up for signal registration.

values of the cross section for photodetachment [30] are almost the same for the first and second harmonics of the laser radiation. In our case, the second harmonic has been chosen for technical reasons (available optical system and easier adjustment when the radiation is in the visible range). The laser beam diameter is controlled by a diaphragm, mounted on the entrance window of the discharge vessel. The beam energy is measured by a Gentec QE25-LP-H-MB joulemeter positioned at the beam exit window.

The detached electrons are registered with a L-shaped Langmuir probe: a tungsten wire with a length of 10 mm and a radius of 0.2 mm. A probe bias of 30 V above the plasma potential ensures operation of the probe in the electron saturation current part of the probe characteristics. A choke filter tuned at the driving frequency (27 MHz) and two low-pass filters are used to suppress interferences caused by the rf-driving of the discharge. The low-pass filters are with a suitably chosen cut-off frequency such that the registered photodetachment signal is not distorted (the time constant of the filters is chosen to be smaller than the rise time of the signal).

The change in the electron saturation current due to the electrons detached by the laser pulse is recorded by a real-time digital storage oscilloscope. The recorded signals are then transferred to a personal computer for further processing.

3. Comments on the use of the laser photodetachment technique

As is known [30, 31], the determination of the electronegativity n_-/n_e (where n_- is the concentration of the negative ions and n_e is the electron density) by using the laser photodetachment technique in combination with a probe is based on measurements of the increase in the electron saturation current of the probe due to the detachment of electrons from the negative ions ($H^- + h\nu \rightarrow H + e$) caused by irradiating the plasma—with a proper, with respect to the wavelength—laser beam. Probe measurements of the electron density n_e provide the possibility for the determination of the concentration n_- of the negative ions (in absolute values) from the electronegativity n_-/n_e. As has been commented before [30], for ensuring reliability of the results check on the influence of the laser pulse energy and of the laser beam diameter on the photodetachment signal as well as a verification that the photodetachment fraction saturates with the increase in the laser pulse energy should precede the measurements of the electronegativity.

Figure 3 shows the shape of the measured photodetachment signal δI_{ph} for different values of the laser pulse energy density $W = E/S$, the latter being the laser pulse energy E per

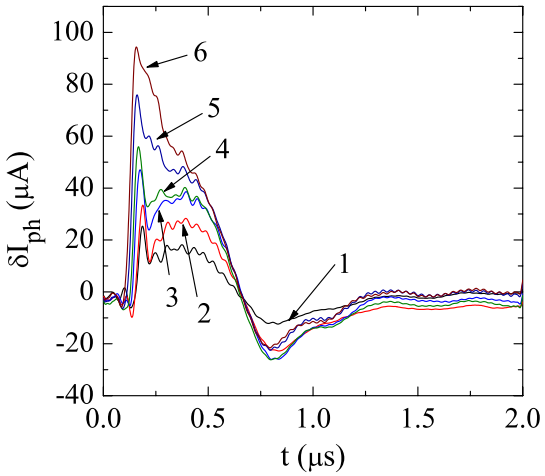

Figure 3. Shape of the photodetachment signal for different values of the laser pulse energy density W; $p = 2$ Pa, $P = 500$ W, $D = 12$ mm. Notation of the signals obtained for different values of W: (1) 8.4 mJ cm^{-2}, (2) 19.4 mJ cm^{-2}, (3) 37.0 mJ cm^{-2}, (4) 47.8 mJ cm^{-2}, (5) 62.7 mJ cm^{-2} and (6) 75.2 mJ cm^{-2}.

unit area ($S = \pi(D/2)^2$ where D is the diameter of the laser beam). Regardless of the disturbances in the signal (the oscillations before its beginning and the noise in its plateau), the typical shape of a photodetachment signal—with a well pronounced plateau in the signal—shows up when the laser pulse energy density is not very high. As has been discussed before, the spike at the beginning of the signal which appears due to a capacitive component in the photodetachment signal [30, 40], when conductive probes are used, should not be considered when the electronegativity n_-/n_e is calculated. Since the photodetachment fraction $\delta n_-/n_-$ (where δn_- is the change in the concentration of the negative ions due to the photodetachment) and, respectively, the electronegativity n_-/n_e should be calculated from the amplitude I_{ph} of the plateau of the signal, figure 3 shows that measurements should not be carried out at the two highest values of the laser pulse energy density because of strong distortion of the photodetachment signal.

Figure 4, where the dependences on the laser pulse energy density of the measured and the calculated photodetachment fractions are compared, also shows that laser pulse energy densities above $W = 50$ mJ cm^{-2} should not be used since they lead to excess electron current (respectively, overestimated negative ion density) due to probe surface ablation [41] showing evidence in a large anomalous noise [41, 42] in the signal. The theoretical curve is calculated according to [30]

$$\frac{\delta n_-}{n_-} = 1 - \exp\left(-\frac{\sigma}{h\nu}W\right), \tag{1}$$

where $h\nu$ is the photon energy and σ [30] is the value of the cross section for photodetachment for the given wavelength of the laser. The normalized measured values of the plateau amplitudes of the signals (figure 3) coincide very well with the theoretical curve excluding the last two highest values just commented. Moreover, the comparison shows that at the value $W = 50$ mJ cm^{-2} of the pulse energy density the photodetachment fraction is saturated, i.e.

$$\frac{\delta n_-}{n_-} = 1, \tag{2}$$

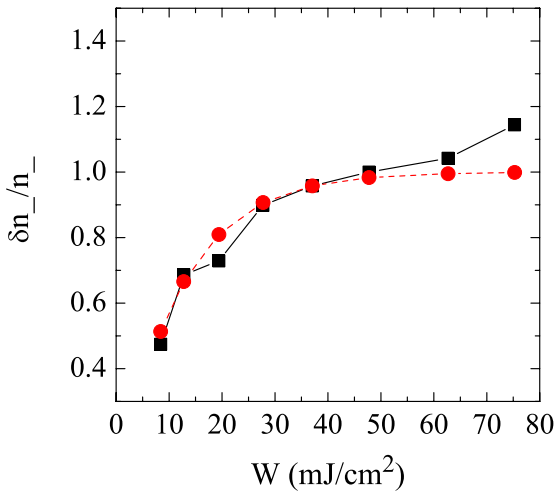

Figure 4. Comparison of the dependence on the laser pulse energy density W of the measured (■, solid curve) and theoretical (●, dashed curve) photodetachment fraction $\delta n_-/n_-$; $p = 2$ Pa, $P = 500$ W, $D = 12$ mm.

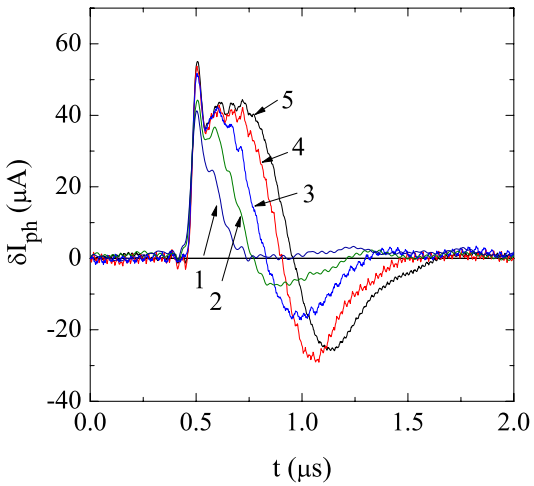

Figure 5. Variation of the shape of the photodetachment signal with changes in the laser beam diameter D; $p = 0.8$ Pa, $P = 500$ W, $W = 37$ mJ cm^{-2}. Notation of the signals obtained for different values of D: (1) 4 mm, (2) 6 mm, (3) 8 mm, (4) 10 mm and (5) 12 mm.

thus reducing the determination of the electronegativity to measuring the ratio

$$\frac{I_{\rm ph}}{I_{\rm e}^{\rm sat}} \equiv \frac{\delta n_{\rm e}}{n_{\rm e}} = \frac{n_-}{n_{\rm e}}, \tag{3}$$

where $I_{\rm e}^{\rm sat}$ is the dc current to the probe at the given probe bias.

The results obtained for the effect of the diameter D of the laser beam on the shape of the signal are presented in figure 5. Diaphragms of different diameters $D = (4–12)$ mm have been used. According to the requirements [30] for choosing a proper diameter of the laser beam, the value of $D = 8$ mm appears to be the smallest one which could be used in our case. Above this value the amplitude of the photodetachment current pulse stays constant (figure 6),

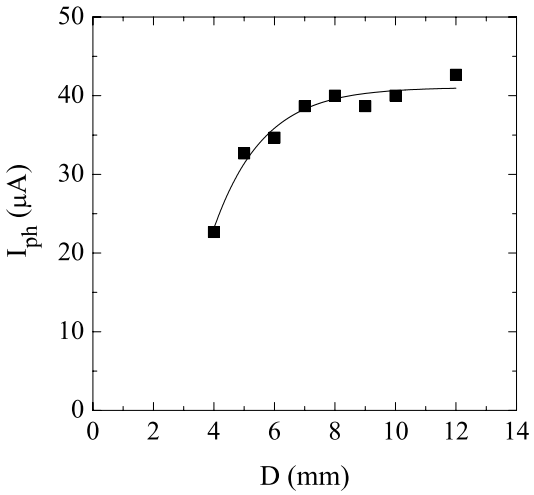

Figure 6. Dependence of the plateau value I_{ph} of the photodetachment signal on the diameter D of the laser beam; $p = 0.8$ Pa, $P = 500$ W, $W = 37$ mJ cm^{-2}.

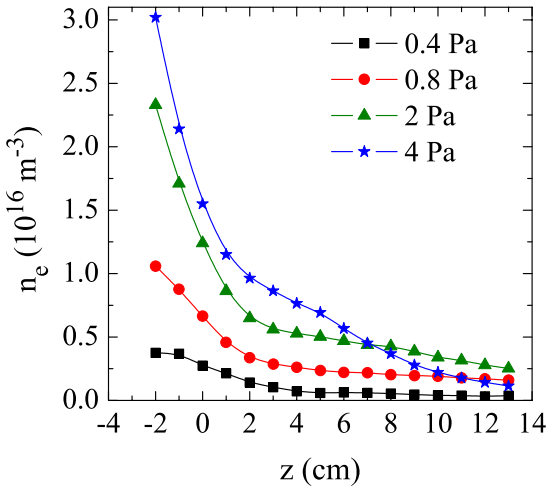

Figure 7. Axial profiles of the electron density at different values of the gas pressure; $P = 500$ W. The position $z = 0$ cm is at the transition between the two chambers.

not depending on the beam diameter. The results presented further on are obtained by using a diaphragm of $D = 10$ mm.

4. Results for the stationary plasma parameters

The results for the stationary plasma parameters—electron density and temperature—shown here are obtained from measurements in the expanding plasma volume of the source by using the SMART probe.

The obtained axial profiles of the electron density (figure 7) are in agreement with previous results [33]. Compared with [33], here the measurements are extended towards lower gas

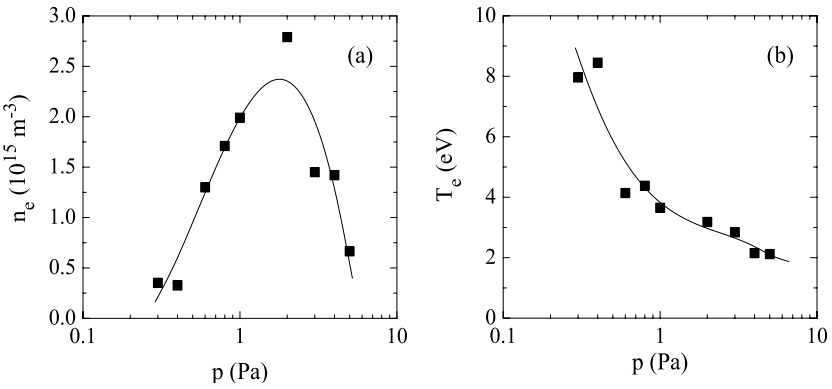

Figure 8. Variation of the electron density (*a*) and temperature (*b*) with the gas pressure at $z = 12$ cm; $P = 500$ W.

pressures. Also the measurements start slightly inside the first chamber (at 2 cm inside the first chamber, before the transition between the two chambers). The electron density n_e decreases away from the driver with a gradient that changes along the discharge length. The strong drop in n_e which starts in the first chamber transfers into a plateau-like region which is more pronounced at higher pressures and continues in the second chamber with a further slight decrease. The behaviour of $T_e(z)$ is also that shown in [33]: a strong axial decrease in T_e in the beginning of the second chamber followed by a further slower decrease. The electron temperature decreases with the gas pressure increase resulting in a higher plasma density (figure 7). However, the latter concerns the gas pressure variation of the plasma density inside the first chamber and in the beginning of the second chamber. The complicated changes in the plasma density with varying gas pressure deep in the second chamber discussed in [33] also appear here. This is shown clearly in figure 8(*a*) where the gas pressure variation of the electron density at the position $z = 12$ cm where the photodetachment measurements are carried out inside the second chamber is presented. With the gas pressure increase, n_e first increases reaching a maximum at about $p = 2$ Pa and then decreases for higher gas pressures. As has been discussed before [33] and also, as the modelling of two-chamber plasma sources developed recently [7, 8] shows, plasma existence in the second chamber of the source is mainly due to particle fluxes from the driver. With the gas pressure decrease the charged particle fluxes increase leading to an increase in the electron density (figure 8(*a*)). However, with the further decrease in the gas pressure the electron density deep inside the second chamber decreases since at low gas pressures the plasma expansion from the first chamber starts from a quite lower value of the electron density (figure 7).

Results for the electron temperature at the position $z = 12$ cm where the photodetachment-technique measurements have been carried out are shown in figure 8(*b*). T_e decreases with the gas pressure increase, which is a general behaviour both in the driver and in the expanding plasma volume.

5. Results for the electronegativity and the concentration of the negative ions

The results for the electronegativity n_-/n_e given here are at the position $z = 12$ cm inside the second chamber. In the measurements, both the gas pressure and the absorbed rf power have been varied, in the ranges $p = (0.3–5)$ Pa and $P = (200–700)$ W, respectively.

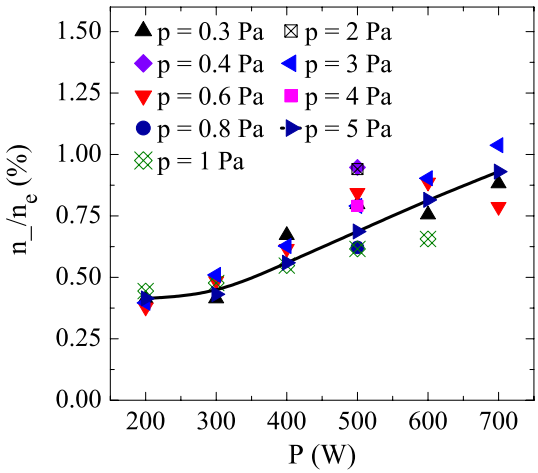

Figure 9. Dependence of the electronegativity on the absorbed rf power for different values of the gas pressure as marked in the figure; $z = 12$ cm.

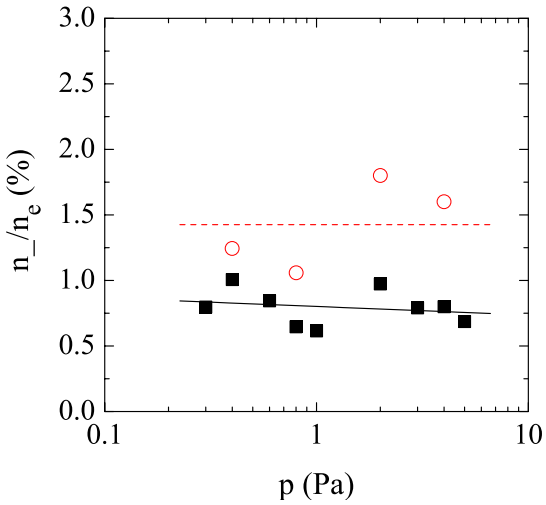

Figure 10. Variation of the electronegativity with the gas pressure; experimental results for $P = 500$ W at $z = 12$ cm shown by closed symbols and solid line and results from theoretical estimations in open symbols and dashed line.

The electronegativity increases with the rf power increase (figure 9) and for $P > 300$ W the variation of n_-/n_e with P could be approximated with a linear dependence ($n_-/n_e \propto P$). Such a dependence is in accordance with a simple balance based on the main reactions: production of vibrationally excited molecules by electron impact and of negative ions by dissociative attachment of electrons to the excited molecules, losses of the negative ions via electron detachment in collisions with atoms and losses of the vibrationally excited molecules at the walls. Such a balance results in $n_-/n_e \propto n_e$ and since n_e is roughly proportional to the absorbed power P, the electronegativity finally scales linearly with P.

The results for the electronegativity obtained for different values of the gas pressure are more curious because the measurements (figure 10) do not show evident variations of n_-/n_e

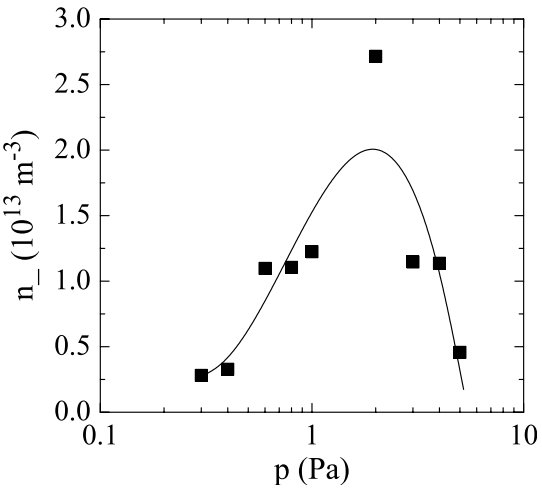

Figure 11. Dependence of the negative hydrogen ion density on the neutral gas pressure; $P = 500$ W, $z = 12$ cm.

with p. In order to have a confirmation of such a result, recent fluid-plasma models of hydrogen discharges [15, 43] were involved in a simplified form. From the model [43] of hydrogen discharges without negative ions taken into account, the concentrations n_j ($j = 1$–3) of the three types of positive ions (H^+, H_2^+ and H_3^+) and of the hydrogen atoms (n_H) and molecules (n_{H_2}) as well as the electron temperature T_e were obtained by solving the balance of H^+, H_2^+, H_3^+ and H (taking into account the particle fluxes to the walls) as a set of equations together with the condition for quasineutrality and the expression for the gas pressure. Ignoring the negative ions at this stage is justified by the low values of the electronegativity measured (figures 9 and 10). The obtained values for n_j, n_H, n_{H_2} and T_e are used for obtaining the concentrations n_ν ($\nu = 0$–14) on the discharge axis ($r = 0$) of the vibrationally excited states of the ground electronic state of the hydrogen molecules according to their balance [15] which accounts for the production of excited molecules via eV and EV collisions and vibrational–translational (V–T) and vibrational–vibrational (V–V) processes and their losses via diffusion and deactivation at the walls; dissociation of H_2 by V–T and V–V relaxation is also included. The obtained local values (on the discharge axis) of n_ν ($\nu = 0$–14), n_j ($j = 1$–3), n_H and T_e are used in a local balance (at $r = 0$) of the negative ions which includes [15] their production via dissociative attachment to vibrationally excited hydrogen molecules and their destruction via electron detachment in collisions with electrons and atoms as well as recombination with the three types of positive ions. The calculations have been carried out with the value of the radius of the quartz tube. The scattering of the theoretical values of the electronegativity (figure 10) is due to using as parameters in the calculations the measured values of the electron density n_e and of the gas pressure p. As figure 10 shows, the calculated and measured values of the electronegativity are in good agreement. Moreover, similar to the experimental results, the theoretical values of n_-/n_e do not show a dependence of the electronegativity on the gas pressure. In addition, the calculated values of the electron temperature coincide very well with the experimental ones.

The experimental results for the electronegativity (figure 10) and those for the electron density (figure 8(*a*)) finally give the pressure dependence of the concentration n_- of the negative ions (figure 11) at the given axial position inside the expanding plasma volume. It shows that n_- peaks up for $p = 2$ Pa. However, it should be stressed that obtaining a maximum

of n_- and, respectively, considering the value of $p = 2$ Pa as an optimum value of the gas pressure regarding the high concentration of the negative ions stems from the given gas pressure dependence of the electron density (figure 8(*a*)), not from a gas pressure dependence of the electronegativity.

6. Conclusions

The study presents experimental results on the electronegativity and the concentration of the negative ions in the expanding plasma region of a two-chamber inductively driven plasma source operating in hydrogen gas in the gas pressure range $p = (0.3–5)$ Pa. The lowest gas pressure values studied approach the pressure range of interest regarding the use of such a type of a source for fusion applications. The measurements show that the electronegativity increases with the rf power absorbed for the discharge maintenance and stays almost constant with the gas pressure variation. Although the latter is curious as a result, it is confirmed by theoretical estimations obtained from a detailed analysis of the particle balance in the discharge. A further extension of the work are experiments currently carried out with a magnetic filter for electron cooling inserted in the expansion plasma volume of the source.

Acknowledgments

Discussions with Professor Dr U Czarnetzki are gratefully acknowledged. The work is within the programme of the Bulgarian Association EURATOM/INRNE (task P2), Project 3.4-Fokoop-BUL/10 26 323 supported by the Alexander-von-Humboldt Foundation and project D01-413 supported by the National Science Fund (Bulgaria) and Sofia University.

References

[1] Speth E *et al* 2006 *Nucl. Fusion* **46** S220
[2] Speth E *et al* 2005 *Fusion Eng. Des.* **74** 279
[3] Bacal M 1989 *Nucl. Instrum. Methods Phys. Res.* B **37–38** 28
[4] Bacal M 2006 *Nucl. Fusion* **46** S250
[5] Riz D and Paméla J 1998 *Rev. Sci. Instrum.* **69** 914
[6] Mizuno T, Kitade Y, Hatayama A, Sakurabayashi T, Imai N, Morishita T and Inoue T 2004 *Rev. Sci. Instrum.* **75** 1760
[7] Kolev St, Shivarova A, Tarnev Kh and Tsankov Ts 2008 *Plasma Sources Sci. Technol.* **17** 035017
[8] Kolev St, Shivarova A, Tarnev Kh and Tsankov Ts 2008 *IEEE Trans. Plasma Sci.* **36** 1390
[9] Haas F A, Lea L M and Holmes A J T 1991 *J. Phys. D: Appl. Phys.* **24** 1541
[10] Holmes A J T 1996 *Plasma Sources Sci. Technol.* **5** 453
[11] Shirai M, Ogasawara M, Koishimine T and Hatayama A 1996 *Rev. Sci. Instrum.* **67** 1085
[12] Kolev St, Lishev St, Shivarova A, Tarnev Kh and Wilhelm R 2007 *Plasma Phys. Control. Fusion* **49** 1349
[13] Franklin R N and Snell J 1992 *J. Phys. D: Appl. Phys.* **25** 453
[14] Franklin R N 2000 *Plasma Sources Sci. Technol.* **9** 191
[15] Paunska Ts, Schlüter H, Shivarova A and Tarnev Kh 2006 *Phys. Plasmas* **13** 023504
[16] Kolobov V I and Economou D J 1997 *Plasma Sources Sci. Technol.* **6** R1
[17] Godyak V 2003 *Plasma Phys. Control. Fusion* **45** A399
[18] Kolev St, Paunska Ts, Shivarova A and Tarnev Kh 2007 *J. Phys.: Conf. Ser.* **63** 012006
[19] Kolev St, Shivarova A and Tarnev Kh 2007 *J. Phys.: Conf. Ser.* **63** 012020
[20] Gorse C, Capitelli M, Bacal M, Bretagne J and Lagana A 1987 *Chem. Phys.* **117** 177
[21] Tabata T and Shirai T 2000 *At. Data Nucl. Data Tables* **76** 1
[22] Celiberto R, Janev R K, Lariechinta A, Capitelli M, Wadehra J M and Atems D E 2001 *At. Data Nucl. Data Tables* **77** 161
[23] York R L, Stevens R R, Leung K N and Ehlers K W 1984 *Rev. Sci. Instrum.* **55** 681

[24] Inoue T, Araki M, Hanada M, Kurashima T, Matsuda S, Matsuda Y, Ohara Y, Okumura Y, Tanaka S and Watanabe K 1989 *Nucl. Instrum. Methods Phys. Res.* B **37–38** 111
[25] Leung K N *et al* 1990 *Rev. Sci. Instrum.* **61** 2378
[26] Leung K N, Hauck C A, Kunkel W B and Walther S R 1990 *Rev. Sci. Instrum.* **61** 1110
[27] Leung K N, Ehlers K M and Bacal M 1983 *Rev. Sci. Instrum.* **54** 56
[28] Fukumasa O, Naiton H and Sakiyama S 1993 *J. Appl. Phys.* **74** 848
[29] Fantz U, Falter H D, Franzen P, Speth E, Hemsworth R, Boilson D and Krylov A 2006 *Rev. Sci. Instrum.* **77** 03A516
[30] Bacal M 2000 *Rev. Sci. Instrum.* **71** 3981
[31] Bacal M 1993 *Plasma Sources Sci. Technol.* **2** 190
[32] Bacal M, Hamilton G W, Bruneteau A M, Doucet H J and Tailler J 1979 *Rev. Sci. Instrum.* **50** 719
[33] Kiss'ovski Zh, Kolev St, Shivarova A and Tsankov Ts 2007 *IEEE Trans. Plasma Sci.* **35** 1149
[34] Djermanova N, Kiss'ovski Zh, Lishev St and Tsankov Ts 2007 *J. Phys.: Conf. Ser.* **63** 012013
[35] Djermanov I, Kolev St, Lishev St, Shivarova A and Tsankov Ts 2007 *J. Phys.: Conf. Ser.* **63** 012021
[36] Kiss'ovski Zh, Kolev St, Shivarova A and Tsankov Ts 2008 *J. Phys.: Conf. Ser.* **113** 012012
[37] Allen J E, Boyd R L F and Reynolds P 1957 *Proc. Phys. Soc.* B **70** 297
[38] Chen F F 1965 *J. Nucl. Energy* C **7** 47
[39] Dimitrova M, Djermanova N, Kiss'ovski Zh, Kolev St, Shivarova A and Tsankov Ts 2006 *Plasma Process. Polym.* **3** 156
[40] Bacal M, Courteille C, Leroy R and Stern R A 1992 *AIP Conf. Proc.* **287** 558
[41] Kajita S, Kado S and Tanaka S 2005 *Plasma Sources Sci. Technol.* **14** 566
[42] Bacal M and Hamilton G W 1979 *Phys. Rev. Lett.* **42** 1538
[43] Koleva I, Paunska Ts, Schlüter H, Shivarova A and Tarnev Kh 2003 *Plasma Sources Sci. Technol.* **12** 597